THE ASTRONOMICAL JOURNAL, 117:1056–1062, 1999 February

PARTICULATE MASS LOSS FROM COMET HALE-BOPP

DAVID JEWITT
Institute for Astronomy, University of Hawaii, 2680 Woodlawn Drive, Honolulu, HI 96822; jewitt@ifa.hawaii.edu
AND
HENRY MATTHEWS
National Research Council of Canada, Herzberg Institute of Astrophysics, 5071 West Saanich Road, Victoria, BC V8X 4M6, Canada; and Joint Astronomy Center, 660 N. A'ohoku Place, Hilo HI 96720; hem@jach.hawaii.edu
Received 1998 September 2; accepted 1998 October 21

ABSTRACT

Large particles may be present in comets in numbers sufficient to dominate the total mass of the coma. These large particles are not readily sensed by conventional (optical - infrared) techniques but are prominent at submillimeter wavelengths. Images taken using a new camera sensitive to submillimeter wavelengths reveal that comet Hale-Bopp was a prodigious source of particulate matter, releasing dust at 2000 metric tons per second when near perihelion and contributing 3×10^{13} kg to the interplanetary dust complex. The dust production rate exceeded that of gas (mostly water) by a factor greater than 5.

Key words: comets: general — comets: individual (Hale-Bopp 1995 O1) — radio continuum

1. INTRODUCTION

Comets are ice dust conglomerates thought to have been formed in the outer solar system 4.5 Gyr ago (Weidenschilling & Cuzzi 1993; Weidenschilling 1997). They have been stored at low temperatures since formation in the Oort cloud and Kuiper Belt repositories. Near perihelion, heating by the Sun causes cometary ices to sublimate, producing an expanding gaseous atmosphere or "coma." Gas drag forces expel solid particles from the nucleus into the coma. Very large particles, from centimeters to decimeters in size, can be ejected against the weak gravity of the nucleus (Whipple 1951; Crifo 1987). Presumably, these large particles are products of agglomerative growth in the protosolar nebula and are local analogues of the dust observed in disks surrounding many young stars (Beckwith et al. 1990; Mannings & Emerson 1994). The cometary grain size distribution is thought to be such that large particles contribute little to the total particulate cross-section but may nevertheless carry the bulk of the particulate mass (McDonnell, Lamy, & Pankiewicz 1991). Evidence for the existence of large, mass-dominant particles has been obtained from dust impacts on spacecraft in the comae of comets Halley (McDonnell et al. 1991) and Giacobini-Zinner (McDonnell et al. 1993), from radar echoes from near-Earth comets (Goldstein, Jurgens, & Sekanina 1984; Harmon et al. 1989, 1997), and from observations of cometary dust trails (Sykes et al. 1986). Submillimeter continuum emission provides another measure of large cometary dust particles (Altenhoff et al. 1989; Jewitt & Luu 1990, 1992; Jewitt 1996; Jewitt & Matthews 1997), but observations at submillimeter wavelengths are technologically challenging and have not yet been widely exploited. The advent of a new submillimeter bolometer array, combined with the appearance of bright comet Hale-Bopp (1995 O1) (Hale & Bopp 1995), provided a fortuitous opportunity to study large cometary particles in unprecedented detail.

2. OBSERVATIONS

An intensive observational campaign was mounted at the James Clerk Maxwell Telescope (JCMT) atop Mauna Kea, Hawaii, triggered by the first millimeter-wavelength continuum detection at 1.3 AU preperihelion (Kreysa et al. 1997; Matthews & Jewitt 1997). JCMT is a 15 m diameter telescope designed to operate in the 350–2000 μm wavelength range. The telescope is protected by an optically opaque Gore-Tex membrane, permitting observations of the comet in full sunlight at small solar elongations. We observed C/Hale-Bopp using linear interpolation from ephemerides provided by B. Marsden. Stability of the pointing was checked periodically through observations of nearby planetary, stellar, and extragalactic sources. Sky subtraction was achieved by beam-switching (generally by 90″) in azimuth. Flux calibration was secured through observations of a set of standard objects (Sandell 1994). The earliest (preperihelion) JCMT observations were taken using the B3 spectral line receiver to measure the 850 μm continuum. The Submillimeter Common-User Bolometer Array (SCUBA) became available at about the time of perihelion (1997 April 1) and was used for all postperihelion work. SCUBA represents an advance over previous submillimeter continuum detectors in two respects: first, whereas earlier detectors had only a single pixel, SCUBA operates simultaneously at 850 μm with 37 pixels and at 450 μm with 91 pixels. Second, each pixel of SCUBA is more sensitive than previous detectors by a factor of 10, largely as a result of its extraordinarily low (75 mK) operating temperature. Combined, these features give SCUBA an observing efficiency advantage of 2 to 3 orders of magnitude, when used for mapping applications. The observations, taken using standard procedures, are summarized in Table 1.

An 850 μm image is shown in Figure 1. SCUBA is diffraction limited to 15″ FWHP (full width at half-power) at 850 μm. SCUBA pixels are separated by a distance comparable to the size of the pixel. Imaging observations were taken using a 64-point "jiggle" pattern to fill the image plane. The coma is highly centrally condensed but with a faint extension in the direction toward the Sun, consistent with preferential dayside emission from the nucleus. A surface brightness profile at 850 μm is shown in Figure 2, along with the beam profile measured from nearly simultaneous observations of Uranus. Solid lines in the figure show a steady state model of the coma in which the surface brightness varies with projected radius, p, in proportion to p^{-1},

TABLE 1

JCMT OBSERVATIONS OF HALE-BOPP

UT Date 1997	R (AU)	Δ (AU)	α (deg)	Receiver	S_{850} (mJy)	C_e ($\times 10^{10}$ m^2)	τ_{850} ($\times 10^{-5}$)	M ($\times 10^{11}$ kg)	t_c ($\times 10^5$ s)	dM/dt (10^5 kg s^{-1})
Feb 9.05.....	1.271	1.840	−30.4	B3	329 ± 96	2.6 ± 0.8	8 ± 2	4.8 ± 1.4	4.67	10 ± 3
Feb 16.98	1.186	1.693	−34.8	B3	464 ± 62	3.1 ± 0.4	11 ± 2	5.6 ± 0.7	4.18	13 ± 2
Mar 9.92	0.997	1.379	−46.0	B3	680 ± 220	2.7 ± 0.9	15 ± 5	5.0 ± 1.6	3.11	16 ± 5
Mar 23.00.....	0.932	1.315	49.1	B3	730 ± 170	2.6 ± 0.6	15 ± 4	4.7 ± 1.1	2.87	16 ± 4
Mar 30.83.....	0.915	1.343	48.3	S	720 ± 50	2.6 ± 0.2	15 ± 1	4.8 ± 0.3	2.91	17 ± 1
Apr 6.92.....	0.920	1.406	45.3	S	730 ± 150	2.9 ± 0.6	15 ± 4	5.3 ± 1.2	3.05	18 ± 4
Apr 26.82	1.023	1.702	32.7	S	609 ± 126	3.8 ± 0.8	13 ± 3	6.9 ± 1.4	3.90	18 ± 4
May 2.23.....	1.062	1.785	30.1	S	500 ± 50	3.4 ± 0.3	11 ± 1	6.3 ± 0.6	4.17	15 ± 2
May 6.21.....	1.103	1.858	27.0	S	437 ± 102	3.3 ± 0.8	10 ± 2	6.1 ± 1.4	4.41	14 ± 3
May 12.22.....	1.161	1.958	23.8	S	482 ± 24	4.3 ± 0.2	11 ± 1	7.8 ± 0.4	4.83	16 ± 1
Jun 14.92.....	1.558	2.456	13.9	S	175 ± 36	2.8 ± 0.6	4.7 ± 1.0	5.1 ± 1.0	6.95	7 ± 2
Jul 6.92.....	1.836	2.687	−14.4	S	149 ± 27	3.1 ± 0.6	4.4 ± 0.8	5.6 ± 1.0	8.26	7 ± 1
Sep 9.92.....	2.644	3.037	−18.8	S	110 ± 14	3.5 ± 0.4	3.9 ± 0.5	6.4 ± 0.8	11.2	6 ± 1
Sep 13.92.....	2.692	3.050	−18.9	S	77 ± 20	2.5 ± 0.6	2.7 ± 0.7	4.5 ± 1.2	11.3	4 ± 1
Oct 13.71.....	3.044	3.154	−18.4	S	24 ± 2	0.88 ± 0.07	0.91 ± 0.07	1.6 ± 0.1	12.5	1.3 ± 0.1
Oct 24.68.....	3.170	3.203	−18.0	S	21 ± 2	0.81 ± 0.08	0.81 ± 0.08	1.5 ± 0.1	12.9	1.2 ± 0.1

NOTE.—R and Δ denote the heliocentric and geocentric distances, α is the Sun-comet-Earth angle, Receiver is the receiver employed (either heterodyne 345 GHz receiver B3 or S = SCUBA bolometer array), S_{850} the flux density (1 mJy = 10^{-29} W m^{-2} Hz^{-1}) measured within the 15.″3 angular beam diameter, C_e the equivalent blackbody cross-section, τ_{850} is the beam-averaged optical depth, M is the dust mass within the projected beam, from eq. (2), t_c is the aperture crossing time. $dM/dt = M/t_c$.

and a convolution with the beam profile has been performed. The effects of anomalous refraction and possible drift of the JCMT during the integration together slightly broaden the beam FWHP relative to the diffraction limit (Fig. 2). Within the uncertainties due to the beam and the sky background subtraction, the steady state model gives a good fit to the data and suggests that the dust production rate was constant on the coma outflow timescale ($\approx$1 day). The surface brightness profile provides no evidence for a pointlike nuclear source or for other discrete sources in the coma (cf. de Pater et al. 1998).

3. INTERPRETATION

The continuum flux density is far too strong to be due to free-free emission from cometary plasma (Jewitt & Luu 1992) or to line emission from cometary molecules (e.g., the CO (3–2) rotational transition at 345 GHz is among the brightest lines and falls within the bandpass of the 850 μm filter but contributes negligibly to the signal). The submillimeter flux density, S_ν (Jy), is instead interpreted as thermal emission from cometary solids and given by

$$S_\nu = B_\nu(T)\left(\frac{C_e}{\Delta^2}\right), \quad (1)$$

where $C_e(\lambda)$ (m^2) is the effective blackbody cross-section (measured at wavelength λ) within the projected beam of the JCMT, Δ (m) is the geocentric distance, and $B_\nu(T)$ (W m^{-2} Hz^{-1} sr^{-1}) is the Planck function evaluated at temperature T (K). The present observations fall in the Rayleigh regime, where the Planck function, $B_\nu(T) = 2kT/\lambda^2$ (k = Boltzmann's constant) is only weakly dependent on the adopted temperature. As a first approximation the temperature is taken to be the local blackbody temperature, $T = 278R^{-0.5}$, where R (AU) is the heliocentric distance. It is well known that submicron grains may be superheated above the blackbody temperature as a result of declining emissivities near the Planck maximum (Williams et al. 1997). However, submicron grains are inefficient emitters of submillimeter radiation, would give a steeper spectral index than is measured in C/Hale-Bopp and are unlikely to contribute much to the submillimeter emission.

The effective cross-section peaks at $C_e(850\ \mu\text{m}) \approx 4 \times 10^{10}$ m^2 (Table 1). This is 30 times the geometric cross-section of a 20 km radius spherical nucleus (Weaver et al. 1997), showing that the nucleus contributes little to the 850 μm radiation. The beam-averaged optical depth of the coma is $\bar{\tau}_{850} = C_e(850\ \mu\text{m})/(\pi p^2)$, where p (m) = 5.6×10^6 (Δ/1 AU) is the linear radius of the projected beam expressed in meters. Table 1 shows that $\tau \ll 1$, meaning that the coma is optically thin at 850 μm and justifying our neglect of radiative transfer. In an optically thin, spherically symmetric, steady state coma the optical depth measured along the line of sight to the nucleus is related to $\bar{\tau}_{850}$ by $\tau_{850}(0) = p\bar{\tau}_{850}/(2\pi r_n)$ (cf. Jewitt 1991). For example, at perihelion, with $r_n = 20$ km, we calculate $\tau_{850}(0) = 9 \times 10^{-3}$. Therefore, our observations suggest that the coma is also optically thin at 850 μm all the way to the nucleus. Of course, the coma of C/Hale-Bopp viewed at high spatial resolution would not be spherically symmetric, and the possibility that some dense dust jets might be locally optically thick cannot be rejected.

The cross-section and the grain mass, M (kg), are related by $C_e(\lambda) = \kappa(\lambda)M$, where $\kappa(\lambda)$ (m^2 kg^{-1}) is the opacity at wavelength λ. The opacity is conventionally written $\kappa(\lambda) = \kappa(\lambda_0)(\lambda_0/\lambda)^\beta$, where λ_0 is a reference wavelength (here taken to be $\lambda_0 = 1$ mm) and β is the spectral index. The opacity is a function of the particle size distribution, composition, and particle shape. Calculations for a wide but physically plausible range of particle compositions and size distributions give $\kappa(1\ \text{mm}) \approx 0.05$ m^2 kg^{-1} (Pollack et al. 1994; cf. Hildebrand 1983; Beckwith et al. 1990), with 90% of the values falling between 0.01 and 0.08 m^2 kg^{-1}. Conducting fractal aggregates (Pollack et al. 1994) and certain amorphous silicates (Agladze et al. 1996) give substantially larger millimeter wavelength opacities. Conducting particles never dominate the submillimeter opacity because of their low cosmic abundance relative to silicates and organics. Infrared spectra of C/Hale-Bopp show prominent features due to

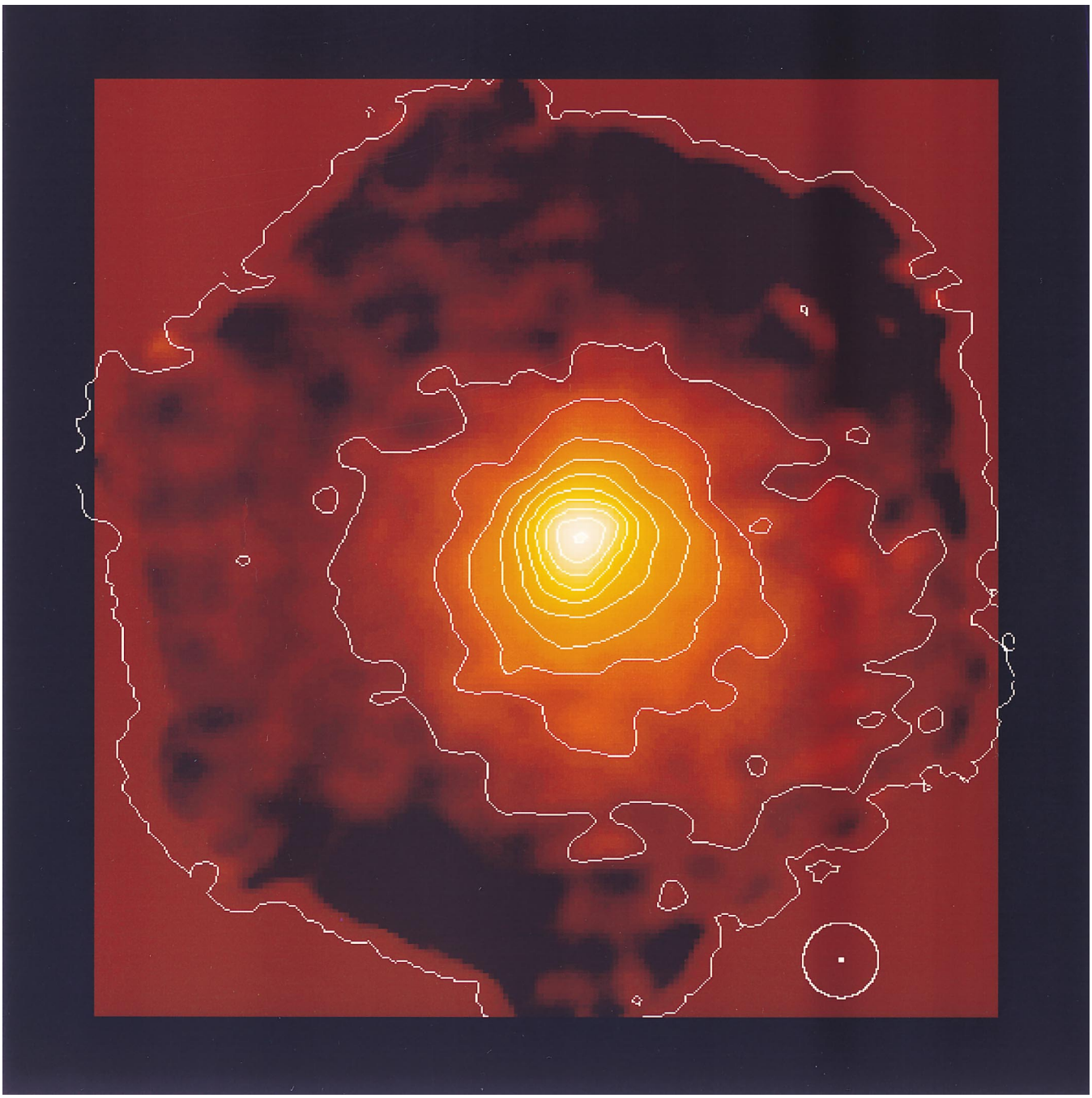

FIG. 1.—Image of C/Hale-Bopp taken 1997 April 6 with the SCUBA bolometer array at 850 μm wavelength. The field of view is 155″ (158,000 km) wide, with north to the top and east to the left. The direction toward the Sun is marked with a white circle. The diameter of the circle equals the 15″.3 resolution of the JCMT. Contours mark surface brightness 10%, 20%, ..., up to 100% of the peak. This image represents 21.3 minutes of integration.

crystalline rather than amorphous olivine (Crovisier et al. 1997). Further, the amorphous silicates measured by Agladze et al. (1996) had spectral indices $\beta > 1.2$, while the spectral index determined from SCUBA multiwavelength observations (Table 2) is significantly smaller, $\beta = 0.60 \pm 0.13$ ($450 \leq \lambda \leq 2000$ μm; Fig. 3). This is formally compatible with $\beta = 0.89 \pm 0.10$ measured in comet Hyakutake (Jewitt & Matthews 1997) and with spectral indices in some (but not all) circumstellar disks (Beckwith et al. 1990). A weighted fit to the BIMA data from Table 2 of de Pater et al. (1998) gives $\beta = 0.0 \pm 0.5$ ($2700 \leq \lambda \leq 3500$ μm), which is also compatible with the JCMT determination within the large uncertainty. (Note that de Pater et al. measured different wavelengths at different times so that temporal variations might affect their measured spectral index. Furthermore, they corrected for the varying geocentric distance, Δ, by scaling their data in proportion to Δ^2. We scaled their data by Δ^1 to correctly account for the extended nature of the C/Hale-Bopp coma). Submillimeter spectral indices $\beta < 1$ are diagnostic of particle sizes greater than 1 mm (Pollack et al. 1994). With $\tau_\lambda(0) \propto \kappa(\lambda) \propto \lambda^{-0.6}$, and taking $\tau_{850}(0) = 9 \times 10^{-3}$, we find $\tau_\lambda(0) = 1$ at $\lambda = 0.33$ μm. While it is not clear that $\beta = 0.6$ holds at wavelengths far outside the submillimeter range, the data allow the possibility that the continuum might become optically thick in the near ultraviolet (cf. Fernandez et al. 1997).

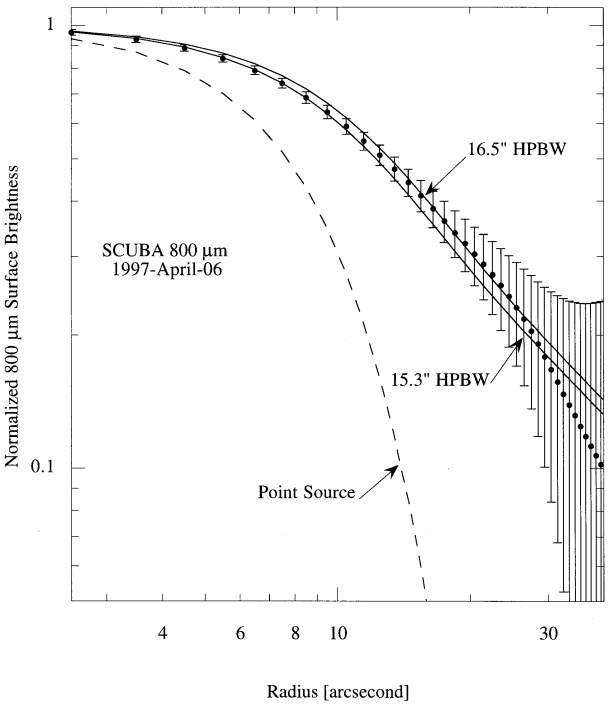

FIG. 2.—Surface brightness profile of C/Hale-Bopp computed from the SCUBA 850 μm image of 1997 April 6. The profile shows the average surface brightness within concentric annuli centered on the brightest pixel in Fig. 1. Error bars on the profile show the effect of uncertainties in the background subtraction. The dashed line shows the point-spread function of the JCMT, determined from a nearly contemporaneous observation of Uranus (angular diameter 4″). Solid lines show models in which the coma surface brightness varies with projected radius, p, as $1/p$ for instantaneous seeing of 15″.3 and 16″.5, FWHM. Two models are plotted to show the effect of small uncertainties in the instantaneous seeing.

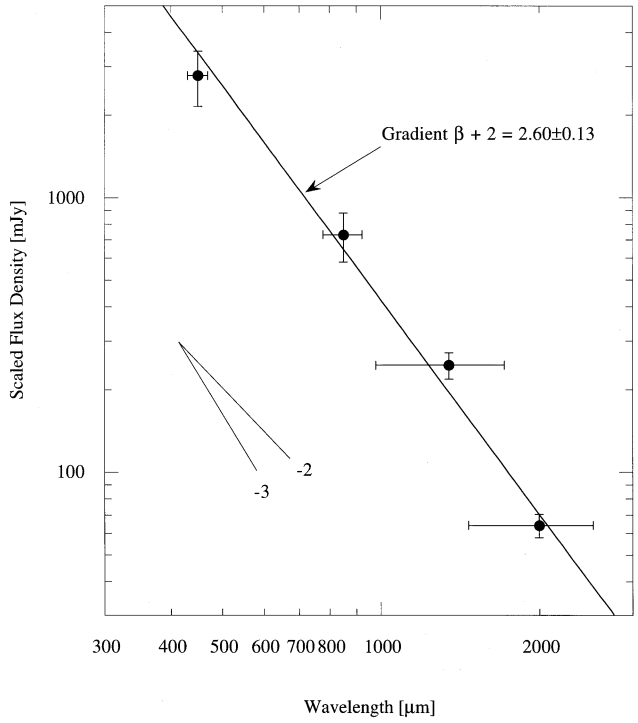

FIG. 3.—Spectrum of C/Hale-Bopp from SCUBA measurements on 1997 April 6. The flux densities have been scaled to a fixed (15″.3) angular aperture size. Horizontal error bars mark the FWHM of the filters employed. Vertical error bars denote 1 sigma uncertainties on the flux densities. Data are taken from Table 2.

Dust masses derived using $\kappa(850\ \mu\text{m}) = 0.055\ \text{m}^2\ \text{kg}^{-1}$ are listed in Table 1. Grains ejected from the nucleus at speed $V(R)$ (ms^{-1}) leave the projected JCMT beam in the "residence time" $t_c = p/V(R)$. An estimate of the mass production rate is obtained by dividing the submillimeter dust mass by the residence time. The calculation of the grain ejection velocity is notoriously difficult, but the key issues can be seen from the following crude treatment. Micron-sized grains are dynamically well coupled to the gas flow and attain terminal speeds close to the gas velocity ($V \approx V_g \approx 1\ \text{km s}^{-1}$ at 1 AU). Very large grains fail to reach the nucleus escape velocity, V_{esc}, and fall back on the nucleus soon after launch (the escape velocity from the nucleus is $V_{\text{esc}} \approx 15\ \text{ms}^{-1}$ for a 20 km radius sphere of density $\rho = 1000\ \text{kg m}^{-3}$). A small subset of the particles with $V \approx V_{\text{esc}}$ can be perturbed by radiation pressure and other forces into temporarily bound orbits. Numerical experiments suggest that such particles are rare and carry only a tiny fraction (10^{-4} to 10^{-2}) of the ejected dust mass (Knollenberg & Kuhrt 1997; Fulle 1997). We do not expect the bound coma to contribute significantly to the measured signal. The symmetric 850 μm light curve of C/Hale-Bopp (Fig. 4) empirically suggests that bound dust is a minor component, since most bound particles would be injected near perihelion, causing a postperihelion brightening that is not observed.

The equation of motion for particles with terminal speeds $V_{\text{esc}} < V < V_g$ is

$$\frac{4}{3}\pi\rho a^3 V \frac{dV}{dr} \approx C_D \pi a^2 \rho_g(r) V_g^2 , \qquad (2)$$

where ρ (kg m^{-3}) is the grain density, a (m) is the grain radius, and C_D is the dimensionless drag coefficient. The gas

TABLE 2

MULTIWAVELENGTH OBSERVATIONS

λ (5 μm)	$\Delta\lambda$ (5 μm)	f (arcsec)	S_ν (mJy)	S_ν^* (mJy)
450	20	8.7	1580 ± 360	2779 ± 633
850	73	15.3	730 ± 150	730 ± 150
1350.....	370	22.3	357 ± 40	245 ± 27
2000.....	530	33.8	141 ± 14	64 ± 6

NOTE.—Taken 1997 April 6. λ and $\Delta\lambda$ are the central wavelength and FWHM of the filter response, respectively. f is the effective beam diameter. S_ν is the measured flux density. S_ν^* is the flux density scaled to a fixed angular aperture size of 15″.3 by $S_\nu^* = S_\nu(15.3/f)$.

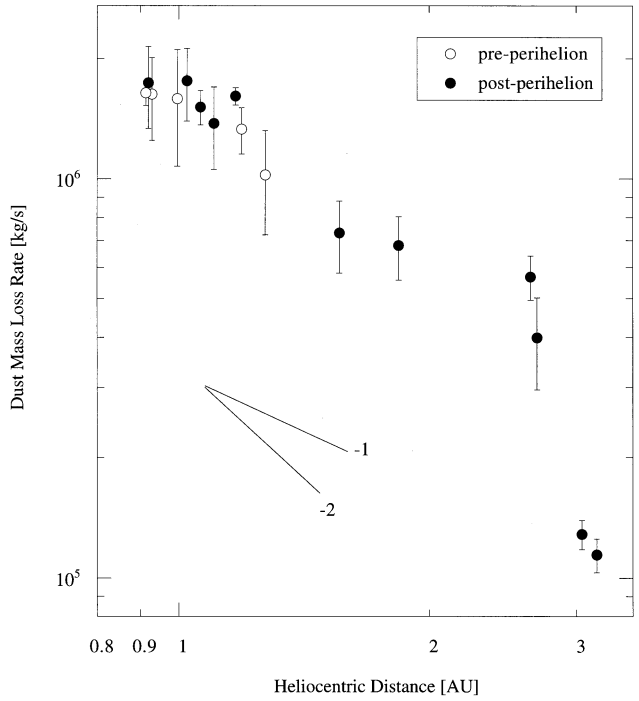

FIG. 4.—Dust mass production rate as a function of heliocentric distance. Open and filled circles denote preperihelion and postperihelion data, respectively. Data are taken from Table 1.

density as a function of distance from the nucleus, r, is

$$\rho_g(r) = \frac{1}{V_g}\left(\frac{r_n}{r}\right)^2 \frac{dm(R)}{dt}, \quad (3)$$

where r_n (m) is the nucleus radius and $dm(R)/dt$ (kg m^{-2} s^{-1}) is the mass sublimation rate per unit area at the surface of the nucleus. Substituting equation (3) into equation (2) and integrating from the nucleus to infinity gives the terminal velocity

$$V = \left[\frac{3 r_n C_D V_g}{2\rho a}\frac{dm(R)}{dt}\right]^{1/2}. \quad (4)$$

Substituting $r_n = 2 \times 10^4$ m, $C_D = 1$, $V_g = 10^3$ ms^{-1}, $\rho = 10^3$ kg m^{-3}, and $dm(1\text{ AU})/dt = 2 \times 10^{-4}$ kg m^{-2} s^{-1} into equation (4) gives

$$V \approx 80\,(1\text{ mm}/a)^{1/2} \quad (5)$$

for the terminal velocity (in ms^{-1}) of a grain of radius a (mm) at 1 AU. This estimate is uncertain because the parameters of the grains and gas flow are not well known. For example, porous particles would have $C_D > 1$ and $\rho < 1000$ kg m^{-3}, leading to higher terminal speeds. The gas flow is also highly variable across the nucleus, again changing the terminal speed for particles of a given size. Detailed hydrodynamic models show that large dust particles are ejected over a wide range of velocities above the escape speed due to the complexities of the gas flow around vents on the nucleus (Gombosi 1986; Crifo 1987; Fulle, Cremonese, & Bohm 1998).

Models specific to comet Halley suggest that millimeter-sized particles were expelled at $V(1\text{ AU}) = 100$ ms^{-1}, close to the nominal value given by equation (5) but with a large uncertainty due to the unknown grain density, drag coefficient, and the complex interaction with near-nucleus jets (Crifo 1987; Gombosi 1986). Terminal velocities for given particle properties and gas flux scale with the square root of nucleus radius (eq. [4]—because the coupling length in the gas is proportional to the nucleus radius), and should be two times larger in C/Hale-Bopp (radius ≈ 20 km) than in P/Halley (radius ≈ 5 km). Indeed, measurements of large dust grains in C/Hale-Bopp beyond 4 AU heliocentric distance suggest high velocities (Fulle et al. 1998).

In view of the uncertainty in the precise value of the ejection velocity, we compute a very conservative limit to the mass-loss rate, by adopting $V(R) = V(1)/R^{0.5}$ ms^{-1} with $V(1\text{ AU}) = 25$ ms^{-1}, for which $V(3\text{ AU}) = 15$ ms^{-1} $= V_{esc}$. This relation underestimates the velocity relative to equation (5) by a factor of 3 and so underestimates the dust mass-loss rate by the same factor. The resulting mass-loss rate is $dM/dt \approx M/\tau_c$, or

$$\frac{dM}{dt} \simeq 105\left(\frac{S_\nu}{1\text{ mJy}}\right)\left(\frac{\Delta}{1\text{ AU}}\right)\left[\frac{V(1)}{1\text{ ms}^{-1}}\right]\left(\frac{\lambda}{1\text{ mm}}\right)^{2+\beta}, \quad (6)$$

also given in Table 1. Perfectly absorbing millimeter-sized ice grains have a lifetime to sublimation of only $\approx 10^4$ s at 1 AU. If ejected at 25 ms^{-1}, these grains would be confined to a central core or halo only 250 km in radius, for which the coma surface brightness profile (Fig. 2) provides no evidence. Therefore, we proceed on the assumption that the submillimeter continuum emanates from solids much less volatile than water ice.

Derived peak dust mass-loss rates near perihelion are $(1.8 \pm 0.4) \times 10^6$ kg s^{-1} (Fig. 4). These values are broadly compatible with others obtained using longer (3 mm) wavelength photometry (Senay et al. 1997; de Pater et al. 1998). For comparison, spectroscopic estimates of the water production rate at perihelion vary from 1.2×10^5 kg s^{-1} (Schleicher et al. 1997) to 3×10^5 kg s^{-1} (Biver et al. 1997, 1999). The larger estimate of water production, augmented by a factor ≈ 1.2 to account for CO (Biver et al. 1997, 1999), yields a conservative lower limit to the dust/gas production ratio, $\psi \geq 5/1$. Comparably large ratios have been determined from submillimeter observations of comets P/Swift-Tuttle ($\psi > 3/1$; Jewitt 1996) and C/Hyakutake ($\psi > 6/1$; Jewitt & Matthews 1997), while $\psi > 10$ was deduced for outbursts in C/Hale-Bopp at 6 AU and P/Halley at 14 AU (Sekanina 1996; Sekanina et al. 1992). While C/Hale-Bopp was extremely productive (with peak water production rates 20 times larger than in P/Halley (Schleicher et al. 1997), its mass-weighted dust/gas ratio was evidently not unusual. These large values exceed the canonical ($\psi \approx 0.1$–1; Newburn & Spinrad 1989) dust-to-gas ratios deduced from optical observations but are compatible with measurements at longer wavelengths. This is a well-known consequence of the fact that optical observations preferentially sample the smaller grains of the cometary dust distribution, since these are more abundant and carry a larger fraction of the optical cross-section than do the mass-dominant larger particles (Li & Greenberg 1998).

The SCUBA observations imply heavy dust-loading of the gas flow in the collisional zone near the nucleus, but the momentum flux in the coma is still clearly dominated by the gas. Predictions of small ($\psi \approx 0.1$) dust/gas ratios made using thermal models (Prialnik 1997) are at variance with

the measurements presented here. The dust production (Fig. 4) is seen to be approximately symmetric about perihelion, with a heliocentric variation following $dM/dt \propto R^{-1.7}$ ($0.9 \leq R \leq 2.5$ AU), while the water production follows $R^{-1.6}$ (Biver et al. 1999). The dust/gas production rate ratio is thus practically constant over this distance range, with a measured ψ that is 50 times larger than predicted. The situation at larger R is less clear, with evidence for a steep drop in dust production provided by the last two measurements at $R \geq 3$ AU (Fig. 4). If real, this drop might be caused by fallback onto the nucleus surface as the terminal velocity of the dominant millimeter-sized particles drops below the nucleus escape speed. Additional postperihelion observations are needed to test this possibility, but in view of the fading of the comet, it seems unlikely that any will be secured.

Whether or not the ratio of the dust to gas production rates is the same as the ratio of dust to gas by mass in the nucleus is an important question with no certain answer. If the nucleus contains particles ("boulders") that are too large to be ejected by gas drag, then the dust/gas production ratio measured in the coma provides only a lower limit to the dust/gas mass ratio in the nucleus. In this sense, $\psi > 5$ provides a strong lower bound to the dust/gas ratio in the nucleus. However, this constraint applies only to the thin upper skin heated by the Sun and the properties of the deep nucleus remain observationally unconstrained.

The recognition of the high refractory content of C/Hale-Bopp and other comets should motivate a revision of those published physical models in which the dust/gas ratio is taken to be $\psi \ll 1$. By underestimating the dust content, Prialnik (1997) overestimates the thermal impact of exothermic phase change in the cometary nucleus, because refractory dust adds mass (and heat capacity) to the nucleus but adds no latent heat. For example, thermal runaways due to exothermic phase change in water ice will be severely damped at $\psi = 5$ compared with $\psi = 1$ or 0.1. Likewise, latent heat transfer in the chemical differentiation model of Flammer, Mendis, & Houpis (1998) will be reduced by a refractory content 10 times higher than these authors assumed, with potentially important consequences for the model results. Recalculation of the models including input parameters suggested by the data would be interesting.

Finally, the total dust mass loss estimated by integrating dM/dt around the orbit (and assuming pre-/post-perihelion symmetry) is $\Delta M = 3 \times 10^{13}$ kg ($R \leq 3$ AU). The total water production rate sets a lower limit to the combined areas of the active vents on the nucleus of the comet. An exposed area 1400 km^2 would be needed to supply water at 3×10^5 kg s^{-1} (cf. Schleicher et al. 1997). Since C/Hale-Bopp showed only muted variations in production rate associated with the rotation of the nucleus, we assume that the active areas are widely distributed over the surface, for a total (dayside + nightside) vent area $A = 2800$ km^2. The total mass loss per orbit then corresponds to a recession of the vent floors by an average distance $\Delta r = \Delta M/(\rho A) \approx 10$ m (assuming bulk density $\rho = 1000$ kg m^{-3}) and to a fractional depletion of the nucleus mass $\Delta M/M \approx 10^{-3}$.

4. SUMMARY

Imaging observations of the submillimeter continuum of comet C/Hale-Bopp with the James Clerk Maxwell Telescope reveal:

1. The measured submillimeter continuum is thermal emission from solid particles in the extended dust coma. The coma is everywhere optically thin at 850 μm.

2. The dust coma surface brightness distribution at 850 μm is well described by a steady state outflow model in which the dust number density varies with the inverse square of the distance from the nucleus. Small deviations from this model indicate preferential sunward ejection of the dust.

3. The spectral index, $\beta = 0.60 \pm 0.13$ ($450 \leq \lambda \leq 2000$ μm), suggests large (1 mm) emitting particles. Similar (small) spectral indices are measured in the circumstellar dust disks of young stars, highlighting the common origin of cometary and circumstellar dust.

4. The perihelion dust mass production rate is $(1.8 \pm 0.4) \times 10^6$ kg s^{-1}, and the total mass lost in solids in the 1997 apparition is $\approx 3 \times 10^{13}$ kg ($R \leq 3$ AU). The ratio of dust to gas mass production rates, $\psi \geq 5/1$, appears constant with respect to heliocentric distance throughout the water sublimation zone.

We thank G. Sandell and W. Holland for help with SCUBA, B. Marsden and D. Tholen for ephemeris advice, and NASA for financial support of this work.

REFERENCES

Agladze, N., Sievers, A., Jones, S., Burlitch, J., & Beckwith, S. 1996, ApJ, 462, 1026
Altenhoff, W. J., Huchtmeier, W. K., Kreysa, E., Schmidt, J., Schraml, J. B., & Thum, C. 1989, A&A, 222, 323
Beckwith, S. V. W., Sargent, A. J., Chini, R. S., & Gusten, R. 1990, AJ, 99, 924
Biver, N., et al. 1997, Science, 275, 1915
Biver, N., et al. 1999, Earth Moon Planets, in press
Crifo, J. F. 1987, in Seventh International Symposium on Materials in Space Environment, ed. T. D. Guyenne (ESA SP-399) (Noordwijk: ESA), 408
Crovisier, J., Leech, K., Bockelee-Morvan, D., Brooke, T. Y., Hanner, M. S., Altieri, B., Keller, H. U., & Lellouche, E. 1997, Science, 275, 1904
de Pater, I., Forster, J., Wright, M., Butler, B., Palmer, P., Veal, J., A'Hearn, M., & Snyder, L. 1998, AJ, 116, 987
Fernandez, Y., et al. 1997, BAAS, 29, 3705
Flammer, K., Mendis, D., & Houpis, H. 1998, ApJ, 494, 822
Fulle, M. 1997, A&A, 325, 1237
Fulle, M., Cremonese, G., & Bohm, C. 1998, AJ, 116, 1470
Goldstein, R., Jurgens, R., & Sekanina, Z. 1984, AJ, 89, 1745
Gombosi, T. I. 1986, in Twentieth ESLAB Symposium on the Exploration of Halley's Comet, ed. B. Battrick (ESA SP-250) (Paris: ESA), 167
Hale, A., & Bopp, T. 1995, IAU Circ. 6187
Harmon, J. K., Campbell, D. B., Hine, A. A., Shapiro, I. I., & Marsden, B. G. 1989, ApJ, 338, 1071
Harmon, J. K., et al. 1997, Science, 278, 1921
Hildebrand, R. H. 1983, QJRAS, 24, 267
Jewitt, D. C. 1991, in Comets in the Post-Halley Era, ed. R. Newburn, M. Neugebauer, & J. Rahe (Dordrecht: Kluwer), 19
Jewitt, D. C. 1996, AJ, 111, 1713
Jewitt, D. C., & Luu, J. X. 1990, ApJ, 365, 738
———. 1992, Icarus, 100, 187
Jewitt, D. C., & Matthews, H. E. 1997, AJ, 113, 1145
Li, A., & Greenberg, J. M. 1998, ApJ, 498, L83
Knollenberg, J., & Kuhrt, E. 1997, BAAS, 29, 1029
Kreysa, E., Altenhoff, W., Haslam, C., & Sievers, A. 1997, IAU Circ. 6555
Mannings, V., & Emerson, J. P. 1994, MNRAS, 267, 361
Matthews, H., & Jewitt, D. 1997, IAU Circ. 6566
McDonnell, J., Lamy, P., & Pankiewicz, G. 1991, In Comets in the Post-Halley Era, ed. R. Newburn, M. Neugebauer, & J. Rahe (Dordrecht: Kluwer), 1043
McDonnell, J., et al. 1993, Nature, 362, 732
Newburn, R., & Spinrad, H. 1989, AJ, 97, 552
Pollack, J. B., Hollenbach, D., Beckwith, S., Simonelli, D. P., Roush, T., & Fong, W. 1994, ApJ, 421, 615
Prialnik, D. 1997, ApJ, 478, L107

Sandell, G. 1994, MNRAS, 271, 75
Schleicher, D. G., Lederer, S. M., Millis, R. L., & Farnham, T. L. 1997, Science, 275, 1913
Sekanina, Z. 1996, A&A, 314, 957
Sekanina, Z., Larson, S., Hainaut, O., Smette, A., & West, R. 1992, A&A, 263, 367
Senay, M., et al. 1997, BAAS, 29, 1034
Sykes, M., Lebofsky, L., Hunten, D., & Low, F. 1986, Science, 232, 1115
Weaver, H., et al. 1997, Science, 275, 1900
Weidenschilling, S., & Cuzzi, J. 1993, in Protostars and Planets 3, ed. J. Lunine (Tucson: Univ. Arizona Press), 1031
Weidenschilling, S. 1997, Icarus, 127, 290
Whipple, F. L. 1951, ApJ, 113, 464
Williams, D., et al. 1997, ApJ, 489, L91